High-Performance Quasi-Solid-State Pouch Cells Enabled by in situ Solidification of a Novel Polymer Electrolyte

Qingwen Lu, Changhong Wang, Danni Bao, Hui Duan, Feipeng Zhao ⓘD, Kieran Doyle-Davis, Qiang Zhang, Rennian Wang, Shangqian Zhao, Jiantao Wang*, Huan Huang*, and Xueliang Sun* ⓘD

Conventional lithium-ion batteries (LIBs) with liquid electrolytes are challenged by their big safety concerns, particularly used in electric vehicles. All-solid-state batteries using solid-state electrolytes have been proposed to significantly improve safety yet are impeded by poor interfacial solid–solid contact and fast interface degradation. As a compromising strategy, in situ solidification has been proposed in recent years to fabricate quasi-solid-state batteries, which have great advantages in constructing intimate interfaces and cost-effective mass manufacturing. In this work, quasi-solid-state pouch cells with high loading electrodes (≥ 3 mAh cm^{-2}) were fabricated via in situ solidification of poly(ethylene glycol)diacrylate-based polymer electrolytes (PEGDA-PEs). Both single-layer and multilayer quasi-solid-state pouch cells (2.0 Ah) have demonstrated stable electrochemical performance over 500 cycles. The superb electrochemical stability is closely related to the formation of robust and compatible interphase, which successfully inhibits interfacial side reactions and prevents interfacial structural degradation. This work demonstrates that in situ solidification is a facile and cost-effective approach to fabricate quasi-solid-state pouch cells with both excellent electrochemical performance and safety.

1. Introduction

With the advent of portable consumer electronics has come the rise of conventional Li-ion batteries (LIBs) with carbonate-based liquid electrolytes (LEs), as long-range electric vehicles become even more widespread, the demands placed on such cells will become even greater. However, LIBs are challenged by a series of safety issues, including electrolyte leakage, gas formation, and even fire or explosion, which is primarily due to the use of flammable solvents.[1] Furthermore, state-of-the-art LIBs are approaching their specific energy limits, a key cause of range anxiety for electric vehicles.[2,3] Therefore, improving the safety and energy density of LIBs are two important and urgent tasks in the field of energy storage.

To improve the energy density, graphite, a commonly used anode material in LIBs, is anticipated to be replaced by high-capacity anodes, including silicon and Li metal.[4–7] Unfortunately, the commercialization of the lithium metal anode has been challenged by lithium dendrite growth as well as a low coulombic efficiency (CE) during charge/discharge cycles. Comparatively, graphite–silicon composite (Gr-Si) anodes are widely used for developing next-generation LIBs, which demonstrate not only much-improved energy density but also significantly enhanced safety.[6,7] On the contrary, Ni-rich cathodes (e.g., $LiNi_{0.8}Mn_{0.1}Co_{0.1}O_2$ and NMC811) are important cathode materials for developing next-generation LIBs with high-energy density.[8,9] It can deliver a high specific capacity of ~ 200 mAh g^{-1} with a high average discharge potential of ~ 3.8 V versus Li$^+$/Li, resulting in a substantial energy density increase of more than 30% compared with traditional cathode materials such as LiCoO$_2$ and LiFePO$_4$ (based on the cathode material only). However, the electrochemical performance of NMC811 is challenged by continuous interface degradation.[10–12] As such, constructing an intimate and compatible interface for high-capacity NMC811 is crucial for battery life.

To improve battery safety, solid-state electrolytes have been proposed to replace flammable liquid electrolytes.[13,14] In recent years, various solid-state electrolytes (SSEs) have been developed, including sulfides,[15,16] oxides,[17,18] halides,[19,20] anti-perovskites,[21] and polymer electrolytes (PEs).[22–25] Some of their ionic conductivity is even higher than that of liquid electrolytes, such as $Li_{10}GeP_2S_{12}$ exhibits an extremely high ionic conductivity even at room temperature (generally of the order of 10^{-2} S cm^{-1}).[26] Compared with inorganic SSEs, PEs have greater advantages in device integration, constructing intimate and chemically compatible interfaces, low cost, and good flexibility. In situ polymerization is one simple and high-efficient strategy to fabricate PEs.[27–30] By injecting a precursor solution that is formed by liquid

Dr. Q. Lu, Dr. C. Wang, D. Bao, H. Huang
Glabat Solid-State Battery Inc., 700 Collip Circle, London ON N6G 4X8, Canada
E-mail: hhuang@glabat-ssb.com
Dr. Q. Lu, Dr. C. Wang, Dr. H. Duan, Dr. F. Zhao, K. Doyle-Davis, S. Zhao, Prof. X. Sun
Department of Mechanical and Materials Engineering, University of Western Ontario, London ON N6A 5B9, Canada
E-mail: xsun9@uwo.ca
Q. Zhang, R. Wang, S. Zhao, Prof. J. Wang
China Automotive Battery Research Institute Co, Ltd, Beijing 101407, China
E-mail: wangjt@glabat.com
ⓘD The ORCID identification number(s) for the author(s) of this article can be found under https://doi.org/10.1002/eem2.12447.

DOI: 10.1002/eem2.12447

electrolytes, low-viscosity monomers and initiators into a battery, all the pores in the electrodes are filled with the precursor solution. After thermal polymerization, the precursor solution becomes a quasi-solid, forming an intimate interface between electrodes and electrolytes. Thanks to its simplicity and viability, in situ polymerization has been widely adopted to develop quasi-solid-state batteries. However, most previous work on in situ solidification is based on coin cells, in situ solidification based on practical pouch cells has seldomly been reported.[31]

In this work, we fabricate a quasi-solid-state NMC811|Gr-Si pouch cell via in situ solidification of poly(ethylene glycol)diacrylate-based polymer electrolytes (PEGDA-PEs). Because of the low viscosity of the initial precursor solution, PEGDA-PEs perfectly fill all pores and voids in high-loading electrodes ($\geq$3 mAh.cm^{-2}). In addition, the strong interfacial interaction between PEGDA-PEs and NMC811 and Gr-Si electrodes not only provides fast interfacial lithium-ion transport but also significantly improves interfacial stability. As a result, quasi-solid-state NMC811|Gr-Si pouch cells demonstrate impressive electrochemical performance. Moreover, the PEGDA monomer is inexpensive and in situ solidification technology is simple, facile, and cost-effective. Thus, we believe this work would make a considerable impact in the field of solid-state batteries.
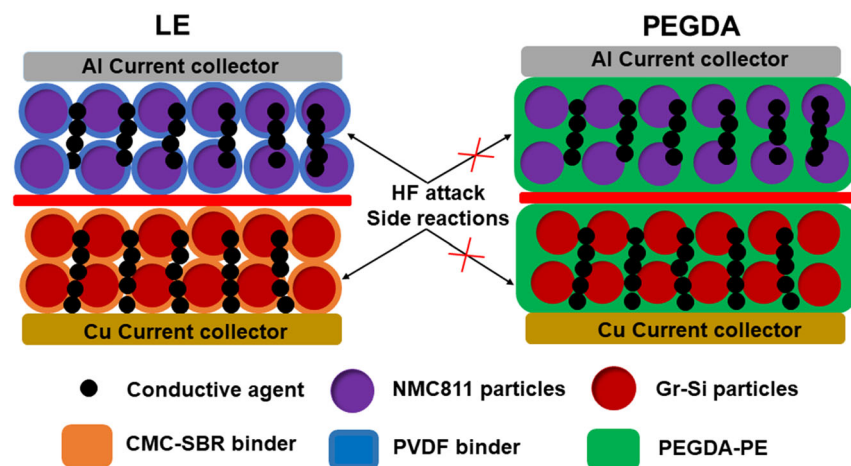
2. Results and Discussion

The process flow of in situ solidification of PEGDA-PE is presented in Figure S1, Supporting Information. 6 wt% PEGDA monomer and 0.2 wt% AIBN thermal initiator was dissolved in LEs and the resultant precursor solution was then injected into an NMC811|Gr-Si pouch cell. After thermal treatment at 60 °C for 12 h, in situ solidified PEGDA-based polymer electrolyte (PEGDA-PE) was formed in pouch cells. The as-prepared colorless, translucent PEGDA-PE exhibits a stable solid with no fluidity (Figure S2, Supporting Information). After solidifying in the pouch cells, the 3D cross-linked network of the PEGDA acts as an internal scaffold to enable better contact between the electrolyte and electrodes, as illustrated in **Figure 1**. The generated PEGDA-PE demonstrates a strong interfacial adhesion with both electrodes. Moreover, a dense protective film is formed on the surface of both electrodes, inhibiting the side reactions between the electrode and the electrolyte. This protective film also protects the electrodes from structural damage during the lithiation–delithiation process, particularly in the case of high-loading NMC811 electrodes. Furthermore, the in situ solidification strategy is facile, low cost, and fully compatible with the conventional roll-to-roll manufacturing process.

Figure 1. Schematic diagram of the electrode-electrolyte interface within the pouch cells with LEs and PEGDA-PEs.

Figure 2. a) FT-IR spectra of PEGDA-based precursor solution before and after thermal polymerization. b) TGA of LE and in situ solidified PEGDA-PE. c) Arrhenius plots of the ionic conductivity of LE and PEGDA-PE with different temperatures. d) Cyclic voltammograms of LE and in situ solidified PEGDA-PE on C65-coated Al working electrode at a scan rate of 1 mV s^{-1}.

The free-radical polymerization reaction of the PEGDA-PE was elucidated by FTIR spectroscopy. As shown in **Figure 2**a, the peak located at 1637 cm^{-1} in the precursor solution is assigned to the stretching vibration of C=C bonds of the PEGDA monomer (Figure S3, Supporting Information), which disappears after the free-radical polymerization, indicating that the PEGDA monomer was fully polymerized and formed a cross-linked PEGDA polymer network. We also confirm that the PEGDA had polymerized on the surface of the NMC811 electrode by FTIR (Figure S4, Supporting Information). Thermal gravimetric analysis (TGA) was also performed to analyze the thermal stability of PEGDA-PEs (Figure 2b). Conventional LEs
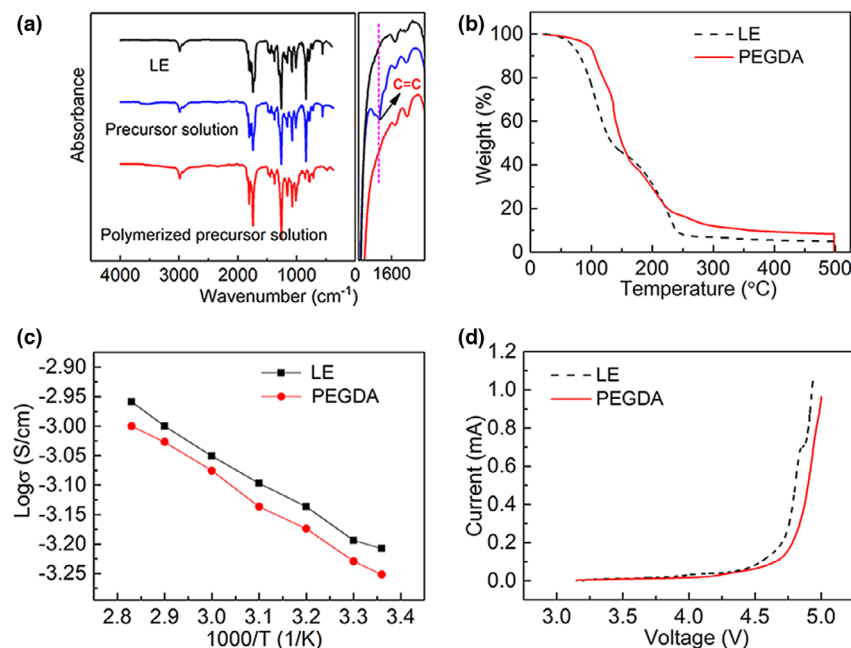
readily evaporate at 60 °C because of the low boiling temperature of the carbonate solvent. In sharp contrast, the PEGDA-PE shows excellent thermal stability to temperatures above 100 °C, which can be attributed to the heat resistance of the cross-linked PEGDA polymer skeleton and their immobility to volatile solvents. The high thermal stability of PEGDA-PEs is of great significance for the safety of NMC811|Gr-Si pouch batteries. Figure 2c shows the temperature dependence of the ionic conductivities of the PEGDA-PEs in comparison with that of conventional LEs. PEGDA-PEs with a separator has a high ionic conductivity of 5.6×10^{-4} S cm^{-1} at 25 °C, which is slightly lower than that of a commercial separator soaked in liquid electrolyte (6.2×10^{-4} S cm^{-1} at 25 °C). The slight decrease in ionic conductivity is related to the restricted ionic motion caused by the cross-linked PEGDA chain. The lithium-ion transference number (t_{Li}^+) was measured by combining the method of DC polarization and AC impedance using the Li/Li symmetric cell (Figure S5a,b, Supporting Information). The t_{Li}^+ of PEGDA-PE is 0.33, which is slightly smaller than that of LE (0.38). This is attributed to greater coordination between Li$^+$ and anions and the polymer matrices. The activation energy was calculated based on the

Arrhenius plot (Figure S5c,d, Supporting Information). The PEGDA-PE has a larger activation energy (11.32 kJ mol^{-1}) than LE (9.26 kJ mol^{-1}), which corresponds to the slightly lower ionic conductivity of PEGDA-PE than that of LE. The electrochemical stability window (ESW) of an electrolyte is a crucial parameter to its compatibility with electrode materials. The ESW was tested with a Li|Electrolyte|C65-coated Al cell. Our previous work[32] has confirmed that using the C65-coated Al electrode as a working electrode is more reliable than just using pure Al foil because the conductive carbon coating enlarges the contact area between electrolytes and electrodes. The ESW results in Figure 2d show that PEGDA-PE can tolerate a voltage over 4.75 V (vs. Li$^+$/Li) while its liquid counterpart begins to degrade at 4.5 V (vs. Li$^+$/Li), demonstrating that PEGDA-PE possesses better oxidation stability against high-voltage cathodes such as NMC811. This improvement is due to the ability of the cross-linked long-chain PEGDA skeleton to immobilize organic solvents and Li salts in the liquid electrolyte, thus significantly suppressing interfacial side reactions.

Next, the cycling performance of in situ solidified PEGDA-PEs was evaluated in single-layer pouch cells with high-loading NMC811 (17.1 mg cm^{-2}) and Gr-Si (8.02 mg cm^{-2}). The pouch cells were charged/discharged in the voltage range of 2.8–4.2 V at a constant current of 0.1 C (1C = 200 mA g^{-1}) rate for the initial three cycles, and then were cycled at 0.5C. The pouch cell with in situ solidified PEGDA-PEs exhibits a discharge capacity of 170.8 mAh g^{-1} and an initial efficiency of 81.03% in the first cycle (0.1 C), which is slightly lower than that of LE counterparts. However, the pouch cell (NMC811|PEGDA-PE|Gr-Si) reveals ultra-stable cycling performance with a high-capacity retention of 82.2% after 500 cycles at 0.5C (**Figure 3a**). The average Columbic efficiency is as high as 99.8% over 500 cycles. In sharp contrast, the pouch cell with conventional LE suffers from fast capacity decay. The capacity retention is 76.9% after 386 cycles. The much-improved cycling stability of quasi-solid-state pouch cells with PEGDA-PEs is ascribed to their better oxidation stability, as proved in Figure 2d. In addition, the quasi-solid-state pouch cells exhibit negligible polarization during long-term cycling (Figure 3b,c).

Furthermore, the NMC811|Gr-Si single-layer pouch cell with PEGDA-PE shows a more stable cycling performance than LE at a high cut-off voltage of 4.4 V (Figure S6, Supporting Information). The pouch cell with in situ solidified PEGDA-PEs exhibits a discharge capacity of 177.7 mAh g^{-1} at 0.5C and an initial efficiency of 80.4% in the first cycle (0.1 C), which is slightly lower than that of LE counterparts (179.8 mAh g^{-1}, 81.3%). The much-improved cycling stability of quasi-solid-state pouch cell with PEGDA-PE at 4.4 V is ascribed to their better oxidation stability than LE.

The rate capability of the NMC811|Gr-Si pouch cells with both liquid electrolyte and PEGDA-PE was compared from 0.1 C to 2.0 C at
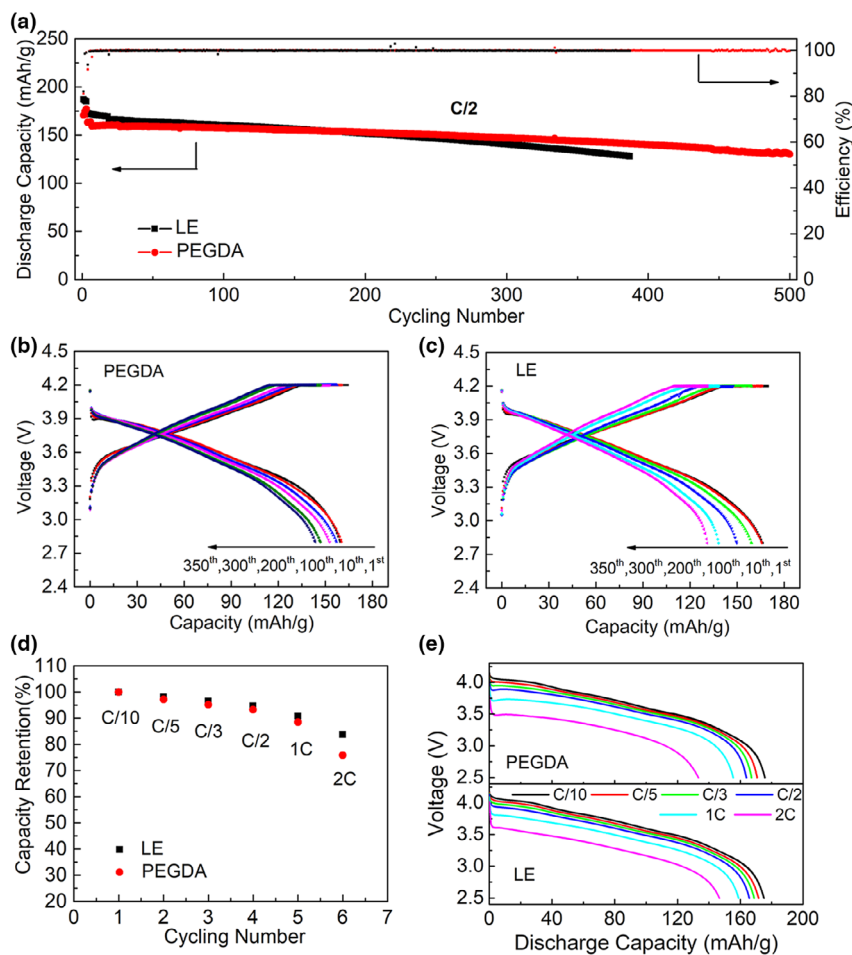

Figure 3. a) Long-term cycling performance of NMC811|LE|Gr-Si and NMC811|PEGDA-PE|Gr-Si single-sheet pouch cells at 0.5C; b, c) Relative charge–discharge profiles of NMC811|PEGDA-PE|Gr-Si and NMC811|LE|Gr-Si single-sheet pouch cells at different cycles. d) Rate performance of NMC811|LE|Gr-Si and NMC811|PEGDA-PE|Gr-Si single-sheet pouch cells at 25 °C; d, e) Relative charge–discharge profiles of NMC811|PEGDA-PE|Gr-Si and NMC811|LE|Gr-Si single-sheet pouch cells at different rates.

room temperature (Figure 3d), and the corresponding charge/discharge profiles are present in Figure 3e. Both pouch cells deliver a high reversible capacity at a relatively low current density (below 0.5C) and their average discharge plateaus gradually decrease with the increasing current density. The slightly reduced discharge capacity of the quasi-solid-state pouch cell at 2.0 C is attributed to its slightly lower ionic conductivity, as evaluated in Figure 2c.

To further confirm the practical applicability of the in situ solidified PEGDA-PE with the industrial standards, we constructed multilayer pouch cells with a large capacity of 2.0 Ah using NMC811, Gr-Si, and PEGDA-PEs (or conventional LEs). Again, PEGDA-PE-based quasi-solid-state pouch cells demonstrated much better cycling stability than LE counterparts (**Figure 4**a). After 550 cycles, a high-capacity retention of 82.3% is kept. Under the same condition (1.0 C), the LE-based multilayer pouch cells exhibit shows a capacity retention of 58.9%. The outstanding performance of Ah-level quasi-solid-state pouch cells with PEGDA-PEs indicates that this facile in situ solidification protocol is very promising for practical battery products with much-improved electrochemical performance but low cost.

Electrochemical impedance analysis was further performed to understand the interfacial ion transport kinetics between the electrode and PEGDA-PEs. The EIS plots of NMC811|PEGDA-PE|Gr-Si and NMC811|LE|Gr-Si single-layer pouch cells after 3 cycles and cycled 330 times are shown in Figure S7, Supporting Information. An equivalent circuit model (Figure S8, Supporting Information) is used to fit EIS results to obtain the bulk resistance (R_1), electrolyte/anode interface resistance (R_2), and electrolyte/cathode interface resistance (R_3).[33] The values of impedance parameters obtained from the simulation results are listed in Table S1, Supporting Information. While the two cells show comparable cycling for the lifetime of the cell, the liquid electrolyte containing cell experiences "roll over" significantly earlier than that of the PEGDA

containing cell. With the aid of electrochemical impedance spectroscopy, we can see that the PEGDA-PE cell has higher initial resistances after 3 formation cycles due to the lower ionic conductivity of the electrolyte (0.57 and 0.25 ohms for the PEGDA and LE cells respectively), after 330 cycles the bulk impedance of the PEGDA containing cell remains unchanged (0.57 ohms). In contrast, the liquid electrolyte cell impedance has nearly quadrupled (1.02 ohms). This impedance growth throughout cycling is indicative of LE consumption, eventually leading to the death of the cell, which is evidently prevented by the PEGDA-PE electrolyte.

Furthermore, a post-mortem analysis by scanning electron microscopy (SEM) was carried out to investigate the interface evolution of both NMC811 and Gr-Si electrodes after 3 cycles and 330 cycles. Before cycling, the fresh cathode and anode surfaces are relatively clean and smooth (Figure S9a,b, Supporting Information). After 3 cycles of formation, a robust interphase layer with a thickness of approximately 2–4 μm was coated on both NMC811 and Gr-Si surfaces (Figure S9c, d, Supporting Information). This interfacial film formed in PEGDA-PE-based pouch cells is dense and uniform (**Figure 5**c,d) while it is more loose and inhomogeneous in LE-based pouch cells (Figure 5a,b). After 330 cycles, the interfacial film in LE-based pouch cells becomes thicker (Figure 5e,f) while the interfacial film in PEGDA-PE-based pouch cells does not change too much (Figure 5g,h), indicating that in situ solidification of PEGDA-PEs is beneficial for constructing robust and dense interfacial interphases in practical pouch cells. This dense and uniform interfacial film is beneficial for suppressing the interfacial side reactions (less gas formation, Video S1, Supporting Information) and mitigating the volume change in Gr-Si and interfacial structure change in NMC811.[34]

X-ray diffraction (XRD) was carried out for pristine NMC811, original Gr-Si anode NMC811 cathodes, and Gr-Si anodes after 330 cycles (Figure S10, Supporting Information). No significant difference in the XRD patterns is detected, indicating good structural reversibility and integrity of the electrodes. Furthermore, transmission electron microscopy (TEM) was performed to investigate the interfacial structural change in electrodes. After 330 cycles, a uniform interphase layer (i.e., CEI and SEI) is covered on NMC811 and Gr-Si surfaces (Figure S11, Supporting Information), effectively suppressing interfacial side reactions and constrained interfacial structural degradation. The post-mortem XRD and TEM analyses further corroborate that the better electrochemical performance of PEGDA-PE-based batteries is attributed to the formation of uniform interfacial interphases.

To examine the chemical information of the robust interfacial films, X-ray photoelectron spectroscopy was performed on the cathode and anode interfaces. The corresponding peak assignment is listed in Table S2, Supporting Information.[35] At the cathode interface, some organic species, RCH_2OCO_2Li, $ROCO_2Li$, and inorganic species LiF, $Li_xPO_yF_z$, are detected (**Figure 6**a–c). It is well known that Li_2CO_3 is not beneficial for interfacial stability and can lead to large interfacial resistance.[36–38] The relative content of Li_2CO_3 in PEGDA-based pouch cells is lower
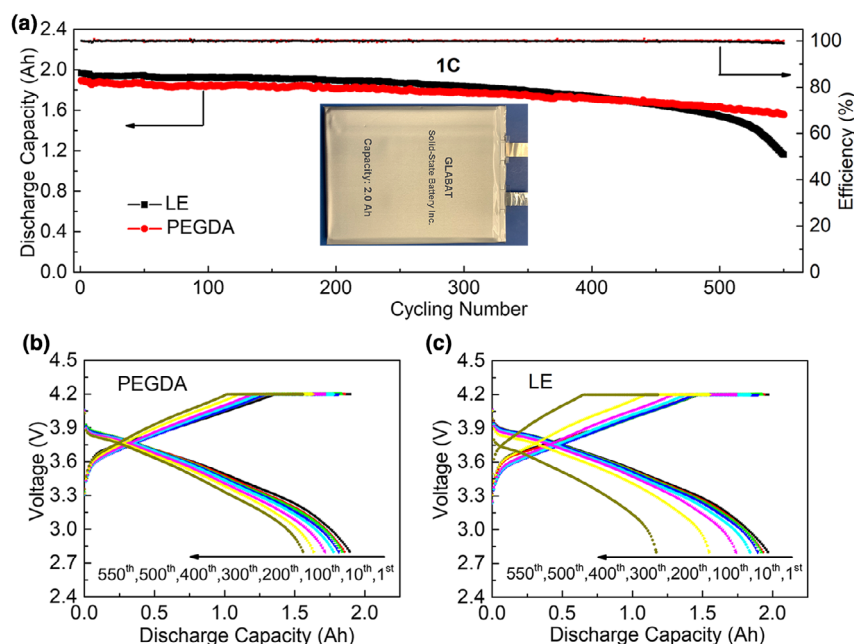

Figure 4. a) Long-term cycling performance of 2.0 Ah NMC811|LE|Gr-Si and NMC811|PEGDA-PE|Gr-Si multilayer pouch cells at 1.0 C rate; b, c) Relative charge–discharge profiles of 2.0 Ah NMC811|PEGDA-PE|Gr-Si and NMC811|LE|Gr-Si multilayer pouch cells at different cycles.

than that in the LE counterparts in O 1 s spectra (Figure 6b), implying that in situ solidified PEGDA-PEs can effectively inhibit the decomposition of LEs and serious side reaction between NMC811 and LEs. More evidently, the intensity of the LiF and $Li_xPO_yF_z$ peaks with PEGDA-PEs after formation and 330 cycles is considerably stronger than those peaks with LEs (Figure 6c). The $Li_xPO_yF_z$ and LiF can serve as an electronic insulator but an ionic conductor, thus effectively preventing the decomposition of LEs and promoting interfacial ion transport.[39,40] At the anode interface, the SEI mainly consists of Li_2CO_3, LiF, $ROCO_2Li$, and RCH_2OCO_2Li.[41–43] In Figure 6d–f, PEGDA-PE-based pouch cells show the strong peaks of $ROCO_2Li$ and RCH_2OCO_2Li, suggesting that the PEGDA-PE promotes the formation of an organic-rich SEI layer.[44–47] In F 1 s spectra (Figure 6f), the $Li_xPO_yF_z$ peak is stronger than in

LE-based cells after 330 cycles, suggesting PEGDA-PE is beneficial for constructing robust SEI with a fast interfacial ion transport kinetics. These facts indicate that the PEGDA-PE can form a stable, flexible SEI layer, thus suppressing electrolyte decomposition and alleviating the volume change in the Gr-Si anode. XPS interfacial analysis confirms that the stable electrochemical performance of quasi-solid-state pouch cells is ascribed to the uniform and robust interface enabled by in situ solidified PEGDA-PEs.

3. Conclusion

In this work, quasi-solid-state pouch cells with high-loading NMC811 and Gr-Si electrodes ($\geq$3 mAh cm^{-2}) were fabricated via in situ solidification of poly(ethylene glycol)diacrylate-based polymer electrolytes (PEGDA-PE). Single-layer pouch cells demonstrate a high-capacity retention of 82.2% after 500 cycles at 0.5C. Practical multilayer pouch cells with a high capacity of 2.0 Ah stably cycle for over 550 cycles with a capacity retention of 82.3%. The impressive electrochemical performance is associated with the formation of robust and compatible interphase, which not only inhibits interfacial side reactions but also prevents interfacial structural degradation. This work demonstrates that in situ solidification is a facile and cost-effective approach to fabricating quasi-solid-state pouch cells with improved electrochemical performance and safety.

4. Experimental Section

Materials: Poly(ethylene glycol)diacrylate (PEGDA, Mn = 700) and 2,2′-Azobis(2-methylpropionitrile) (AIBN) were purchased from Sigma-Aldrich. Lithium Hexafluorophosphate ($LiPF_6$), Ethylene carbonate (EC), diethyl carbonate (DEC), and ethyl methyl carbonate (EMC) solvents were from Dongguan Shanshan Battery Materials Co., Ltd. The carbonate-based liquid electrolyte (LE) contains 1 M $LiPF_6$ solution dissolved in EC/DEC/EMC with a volume ratio of 1:1:1. $LiNi_{0.8}Mn_{0.1}Co_{0.1}O_2$ (NMC811) cathode was obtained from China Automotive Battery Research Institute Co, Ltd. Graphite-Silicon S450 (Gr-Si) composite anode was from Shenzhen BTR New Energy Materials Co., Ltd. Ceramic coated separators (thickness:16 μm) were from Celgard.

Preparation of the precursor solution: The precursor solution was prepared by first dissolving 6 wt% PEGDA in the LE, after the complete dissolution of the monomer, 0.2 wt.% AIBN added was added to the mixture solution. After stirring 30 min, a certain amount of precursor solution was directly injected into the pre-dried full-cell, and then, the aluminum pouch was completely sealed during a vacuum sealer to yield a lithium-ion full-cell before in situ solidification (Table S3, Supporting Information). Absorption of the precursor solution into the separator and electrodes was estimated to occur within 12 h. In situ solidification of pouch cells was done by thermal treatment at 60 °C for 12 h. All procedures for preparing the precursor were carried out in a dry box filled with argon gas.
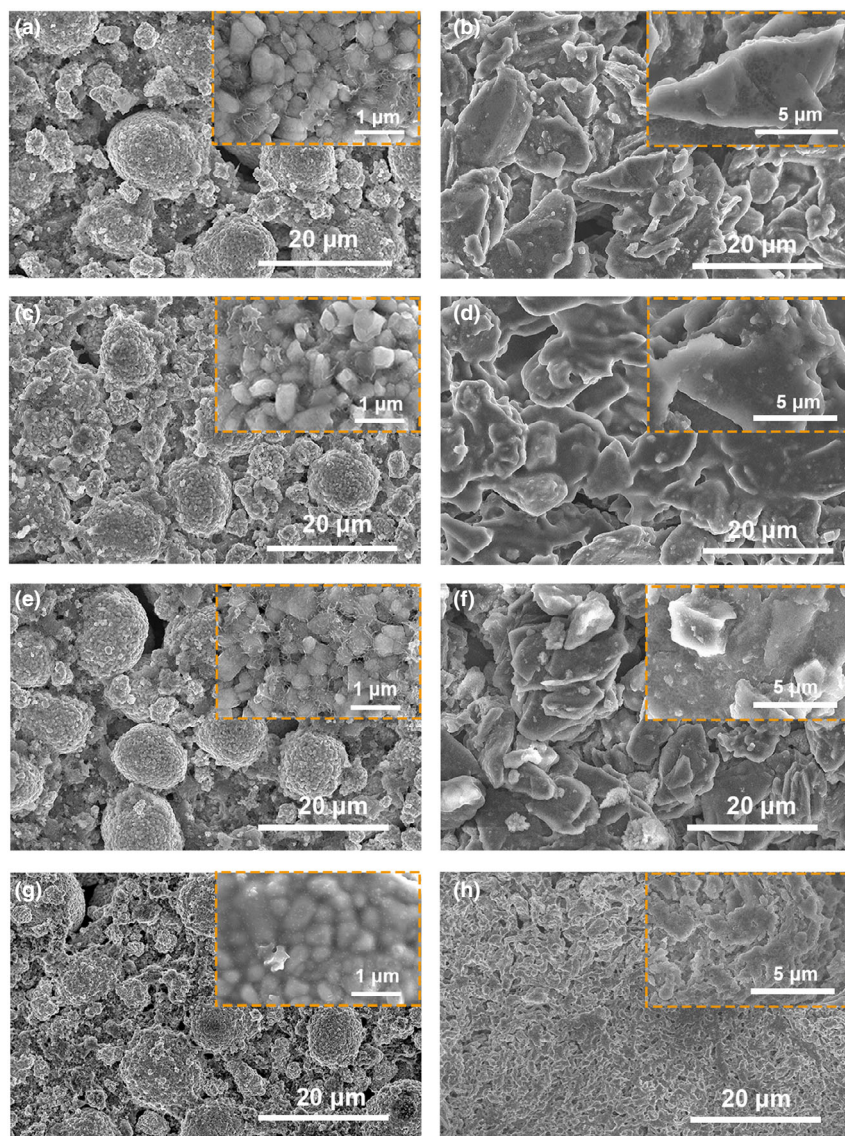

Figure 5. a, b) SEM images of NMC811cathode and Gr-Si anode materials with LEs after 3 cycles formation at 0.1C. c, d) SEM images of NMC811 cathode and Gr-Si anode materials with PEGDA-PE after 3 cycles formation. e, f) SEM images of NMC811cathode and Gr-Si anode materials with LEs after 330 cycles at 0.5C. g, h) SEM images of NMC811 cathode and Gr-Si anode materials with PEGDA-PE after 330 cycles at 0.5C.
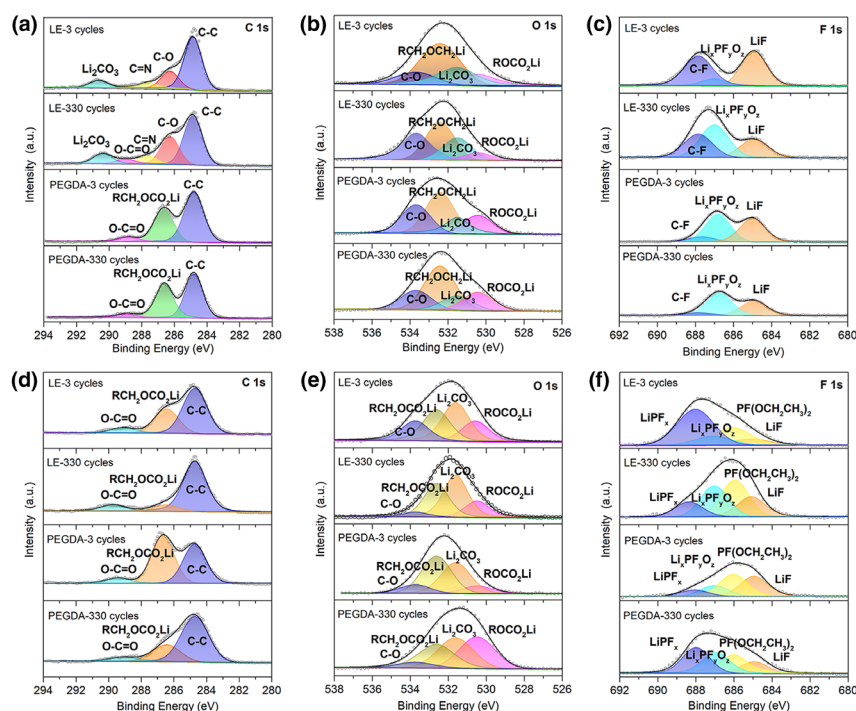
Figure 6. C 1 s, O 1 s, and F 1 s XPS spectra comparison of a, b, c) NMC811 cathodes and d, e, f) Gr-Si anodes taken from NMC811|LE|Gr-Si and NMC811|PEGDA-PE|Gr-Si single-sheet pouch cells after 3 cycles and 330 cycles.

Battery assembly: Single-sheet pouch-type cells with a capacity of 75.24 mAh and multilayer pouch-type cells with a capacity of 2.0 Ah were assembled and dried in a vacuum oven overnight. The single-sheet pouch-type cells were composed of an NMC811 cathode (4.4×5.7 cm^2) and a Gr-Si anode (4.5×5.8 cm^2) with the separator between the cathode and anode (Figure S12, Supporting Information). The multilayer pouch-type cells with a capacity of 2.0 Ah were prepared by China Automotive Battery Research Institute Co, Ltd.

Materials characterizations: The morphology of the NMC811 cathode and Gr-Si anode was examined by field emission scanning electronic microscope (FE-SEM, Hitachi S-4800) and high-resolution transmission electron microscopy (HRTEM) (JEOL 2010 FEG). XRD patterns were recorded using a Bruker D8 diffractometer, using Cu Kα radiation. The free-radical polymerization reaction of the PEGDA was confirmed using an FTIR spectrometer (Bruker Vertex70 instrument). The thermogravimetric analysis (TGA) measurements were performed in a temperature range from room temperature to 500 °C at a heating rate of 5 °C min^{-1} under a nitrogen atmosphere. X-ray Photoelectron Spectroscopy (XPS) was performed using a Thermo Scientific K-Alpha instrument at the University of Toronto. Before FE-SEM and XPS testing, all the electrodes were washed with Dimethyl carbonate (DMC) solvent.

Electrochemical measurements: The ionic conductivity of the electrolytes was determined by EIS measurement using stainless steel|PE|stainless steel symmetric cells with controlled temperature. Lithium-ion transference number (t_{Li}^{+}) measurement was measured by combining EIS and direct current (DC) polarization and AC impedance. The Li|LE|Li and Li|PEGDA|Li symmetric cell was fabricated and polarized by a constant DC voltage of 50 mV. The current was recorded until the current reached a steady state. The initial and steady-state impedances of the cell were also measured by EIS. The electrochemical stability windows (ESWs) were measured using C65-coated Al|PE|Li metal cells. The electrochemical performance of NMC811|Gr-Si pouch cells was assembled in an Ar-filled glove box. The galvanostatic charge–discharge tests were carried out using a Neware battery test system (CT-4008-5V6A, Shenzhen, China) with operating voltages ranging from 2.7 to 4.2 V.

Conflict of Interest

The authors declare no conflict of interest.

Supporting Information

Supporting Information is available from the Wiley Online Library or from the author.

Keywords

[1] J. Kalhoff, G. G. Eshetu, D. Bresser, S. Passerini, *ChemSusChem* **2015**, 8, 2154.
[2] P. G. Bruce, S. A. Freunberger, L. J. Hardwick, J.-M. Tarascon, *Nat. Mater.* **2012**, 11, 19.
[3] M. Armand, J.-M. Tarascon, *Nature* **2008**, 451, 652.
[4] M. Thakur, R. B. Pernites, N. Nitta, M. Isaacson, S. L. Sinsabaugh, M. S. Wong, S. L. Biswal, *Chem. Mater.* **2012**, 24, 2998.
[5] S. Jeong, J.-P. Lee, M. Ko, G. Kim, S. Park, J. Cho, *Nano Lett.* **2013**, 13, 3403.
[6] H.-Y. Lee, S.-M. Lee, *Electrochem. Commun.* **2004**, 6, 465.
[7] P. Li, H. Kim, S.-T. Myung, Y.-K. Sun, *Energy Stor. Mater.* **2020**, 35, 550.
[8] G. L. Xu, X. Liu, A. Daali, R. Amine, Z. Chen, K. Amine, *Adv. Funct. Mater.* **2020**, 30, 2004748.
[9] A. Manthiram, B. Song, W. Li, *Energy Stor. Mater.* **2017**, 6, 125.
[10] K. Beltrop, S. Klein, R. Nölle, A. Wilken, J. J. Lee, T. K.-J. Köster, J. Reiter, L. Tao, C. Liang, M. Winter, *Chem. Mater.* **2018**, 30, 2726.
[11] J. Li, J. Camardese, S. Glazier, J. Dahn, *Chem. Mater.* **2014**, 26, 7059.
[12] K. Märker, P. J. Reeves, C. Xu, K. J. Griffith, C. P. Grey, *Chem. Mater.* **2019**, 31, 2545.
[13] L.-Z. Fan, H. He, C.-W. Nan, *Nat. Rev. Mater.* **2021**, 6, 1003.
[14] Q. Zhao, S. Stalin, C.-Z. Zhao, L. A. Archer, *Nat. Rev. Mater.* **2020**, 5, 229.
[15] C. Wang, J. Liang, Y. Zhao, M. Zheng, X. Li, X. Sun, *Energy Environ. Sci.* **2021**, 14, 2577.
[16] S. Chen, D. Xie, G. Liu, J. P. Mwizerwa, Q. Zhang, Y. Zhao, X. Xu, X. Yao, *Energy Stor. Mater.* **2018**, 14, 58.

[17] H. Huo, J. Liang, N. Zhao, X. Li, X. Lin, Y. Zhao, K. Adair, R. Li, X. Guo, X. Sun, *ACS Energy Lett.* **2020**, *5*, 2156.

[18] H. Huo, J. Gao, N. Zhao, D. Zhang, N. G. Holmes, X. Li, Y. Sun, J. Fu, R. Li, X. Guo, *Nat. Commun.* **2021**, *12*, 1.

[19] X. Li, J. Liang, N. Chen, J. Luo, K. R. Adair, C. Wang, M. N. Banis, T. K. Sham, L. Zhang, S. Zhao, *Angew. Chem.* **2019**, *131*, 16579.

[20] X. Li, J. Liang, X. Yang, K. R. Adair, C. Wang, F. Zhao, X. Sun, *Energy Environ. Sci.* **2020**, *13*, 1429.

[21] J. Dawson, T. Famprikis, K. E. Johnston, *J. Mater. Chem. A* **2021**, *9*, 18746.

[22] H. Zhang, J. Zhang, J. Ma, G. Xu, T. Dong, G. Cui, *Electrochem. Energ. Rev.* **2019**, *2*, 128.

[23] L. Yue, J. Ma, J. Zhang, J. Zhao, S. Dong, Z. Liu, G. Cui, L. Chen, *Energy Stor. Mater.* **2016**, *5*, 139.

[24] W. Zhao, J. Yi, P. He, H. Zhou, *Electrochem. Energ. Rev.* **2019**, *2*, 574.

[25] S.-J. Tan, X.-X. Zeng, Q. Ma, X.-W. Wu, Y.-G. Guo, *Electrochem. Energ. Rev.* **2018**, *1*, 113.

[26] N. Kamaya, K. Homma, Y. Yamakawa, M. Hirayama, R. Kanno, M. Yonemura, T. Kamiyama, Y. Kato, S. Hama, K. Kawamoto, *Nat. Mater.* **2011**, *10*, 682.

[27] Y. G. Cho, C. Hwang, D. S. Cheong, Y. S. Kim, H. K. Song, *Adv. Mater.* **2019**, *31*, 1804909.

[28] D. Zhou, D. Shanmukaraj, A. Tkacheva, M. Armand, G. Wang, *Chem* **2019**, *5*, 2326.

[29] V. Vijayakumar, B. Anothumakkool, S. Kurungot, M. Winter, J. R. Nair, *Energy Environ. Sci.* **2021**, *14*, 2708.

[30] T. Liu, J. Zhang, W. Han, J. Zhang, G. Ding, S. Dong, G. Cui, *J. Electrochem. Soc.* **2020**, *167*, 070527.

[31] X. Li, K. Qian, Y.-B. He, C. Liu, D. An, Y. Li, D. Zhou, Z. Lin, B. Li, Q.-H. Yang, *J. Mater. Chem. A* **2017**, *5*, 18888.

[32] X. Yang, M. Jiang, X. Gao, D. Bao, Q. Sun, N. Holmes, H. Duan, S. Mukherjee, K. Adair, C. Zhao, *Energy Environ. Sci.* **2020**, *13*, 1318.

[33] J. K. Kim, J. Scheers, T. J. Park, Y. Kim, *ChemSusChem* **2015**, *8*, 636.

[34] C. Wang, S. Hwang, M. Jiang, J. Liang, Y. Sun, K. Adair, M. Zheng, S. Mukherjee, X. Li, R. Li, *Adv. Energy Mater.* **2021**, *11*, 2100210.

[35] G. Xu, C. Pang, B. Chen, J. Ma, X. Wang, J. Chai, Q. Wang, W. An, X. Zhou, G. Cui, *Adv. Energy Mater.* **2018**, *8*, 1701398.

[36] H. Kim, F. Wu, J. T. Lee, N. Nitta, H. T. Lin, M. Oschatz, W. I. Cho, S. Kaskel, O. Borodin, G. Yushin, *Adv. Energy Mater.* **2015**, *5*, 1401792.

[37] J. Zhao, Y. Liang, X. Zhang, Z. Zhang, E. Wang, S. He, B. Wang, Z. Han, J. Lu, K. Amine, *Adv. Funct. Mater.* **2020**, *31*, 2009192.

[38] Y. Hu, B. Li, X. Jiao, C. Zhang, X. Dai, J. Song, *Adv. Funct. Mater.* **2018**, *28*, 1801010.

[39] K. Xu, *Chem. Rev.* **2014**, *114*, 11503.

[40] J. Xie, L. Liao, Y. Gong, Y. Li, F. Shi, A. Pei, J. Sun, R. Zhang, B. Kong, R. Subbaraman, *Sci. Adv.* **2017**, *3*, eaao3170.

[41] Y.-C. Lu, A. N. Mansour, N. Yabuuchi, Y. Shao-Horn, *Chem. Mater.* **2009**, *21*, 4408.

[42] T. Dong, J. Zhang, G. Xu, J. Chai, H. Du, L. Wang, H. Wen, X. Zang, A. Du, Q. Jia, *Energy Environ. Sci.* **2018**, *11*, 1197.

[43] J.-N. Zhang, Q. Li, Y. Wang, J. Zheng, X. Yu, H. Li, *Energy Stor. Mater.* **2018**, *14*, 1.

[44] J.-Y. Hwang, S.-J. Park, C. S. Yoon, Y.-K. Sun, *Energy Environ. Sci.* **2019**, *12*, 2174.

[45] Y.-B. He, F. Ning, B. Li, Q.-S. Song, W. Lv, H. Du, D. Zhai, F. Su, Q.-H. Yang, F. Kang, *J. Power Sources* **2012**, *202*, 253.

[46] G. G. Eshetu, X. Judez, C. Li, M. Martinez-Ibañez, I. Gracia, O. Bondarchuk, J. Carrasco, L. M. Rodriguez-Martinez, H. Zhang, M. Armand, *J. Am. Chem. Soc.* **2018**, *140*, 9921.

[47] G. G. Eshetu, T. Diemant, M. Hekmatfar, S. Grugeon, R. J. Behm, S. Laruelle, M. Armand, S. Passerini, *Nano Energy* **2019**, *55*, 327.